Inelastic gas-surface scattering. II. Results

Mark D. Stiles* and John W. Wilkins
Laboratory of Atomic and Solid State Physics, Cornell University, Clark Hall, Ithaca, New York 14853-2501
(Received 18 August 1986; revised manuscript received 29 May 1987)

Helium and molecular-hydrogen scattering from copper is calculated to examine general features of scattering for these systems, especially the quantum mechanics of the scattering process, both for the motion of the particle and the excitations of the lattice. These calculations use an interaction potential chosen to simplify the numerical calculation while retaining the essential physics of the interaction. He-scattering calculations show that these approximations quantitatively reproduce experimental results. Based on this success, we show how the scattering probabilities depend on details of the system like the well depth and the steepness of the potential as well as the assumptions made to simplify the interaction potential. H_2 and D_2 inelastic scattering probabilities show strong enhancement by selective adsorption resonances and overall changes in scattering intensities due to other aspects of the rotational degrees of freedom. Temperature-dependent HD-scattering probabilities show the effect of inelastic scattering on rotationally inelastic scattering and selective adsorption resonances.

I. INTRODUCTION

A recent review of the gas-surface scattering field[1] summarizes the wide variety of systems studied using thermal energy atomic and molecular beams. In this paper we will concentrate on low-mass scattering particles, in particular helium and various isotopes of molecular hydrogen, and on inelastic scattering and the effect of inelastic scattering on elastic scattering in these systems. The specific calculations we report are for He, H_2, D_2, and HD scattering from flat copper surfaces [such as (111) and (100)]. We view these systems as prototypical, allowing generalization of our results to other systems.

Most calculations of inelastic scattering probabilities for these systems are related to the distorted-wave Born approximation. There are four basic approaches: (1) distorted-wave Born approximations based on including only the z-dependent potential in the zeroth-order Hamiltonian,[2-10] (2) distorted-wave Born approximations based on potentials that include the corrugation or translational-rotational coupling in the zeroth-order Hamiltonian,[11-13] (3) extended coupled-channels calculations that are exact calculations on a simplified Hamiltonian, for which the possible final states are restricted in some way,[14-20] and (4) methods related to the last, but leaving out intermediate steps, i.e., calculating the elastic-scattering probability using a self-energy.[21]

In this paper we calculate scattering probabilities for helium and molecular hydrogen using the formal methods developed in its companion paper[20] (hereafter referred to as I) which fall into the third category mentioned in the previous paragraph. Together with the approximations we make for the interaction potential we use these methods to calculate many aspects of the scattering problem which we in turn use to make general statements for atom-surface scattering in the low-mass limit. For readers especially interested in selective adsorption resonances we direct their attention to Sec. III B on molecular-hydrogen scattering.

II. DETAILS OF THE CALCULATIONS

Given the formalism developed in I it is necessary to make some additional choices to perform calculations. Specifically we need a potential and a phonon spectrum. In this section we will discuss the choices made; we have striven to consider simple models with no adjustable parameters so that our assumptions can be tested directly against experiment.

A. The potential

The potential is usually described as due to two contributions, an attractive and a repulsive, which are calculated independently of each other. Far away from the surface the atom is attracted to the surface by a van der Waals attraction that falls off with the inverse cube of the distance from the surface. The other contribution is a repulsive potential due to the atomic electrons overlapping the surface electrons.

Figure 1 shows the potentials for He, H_2, and HD all interacting with a copper surface.[22-26] In Table I we give the parameters for each of the potentials. The helium potential consists of a repulsive part given by

$$V_r(z)=V_0e^{-\alpha z}\ , \tag{2.1}$$

and an attractive part given by

$$V_a(z)=-f(z-z_{vw})\frac{C_{vw}}{(z-z_{vw})^3}\ ,$$
$$f(x)=1-[2(k_cx)^2+2k_cx+1]e^{-2k_cx}\ . \tag{2.2}$$

The function $f(x)$ is a cutoff function that removes the divergence of the usual van der Waals dependence as $z \to z_{vw}$ and in the process softens the attractive potential inside the well minimum. The constant k_c is chosen to give the best comparison with the observed bound states when used in conjunction with a repulsive potential. For helium on copper this potential with a well depth of 5.66 meV supports five bound states.

The hydrogen molecule is more polarizable than helium; in addition both its charge density[24] and its polarizability are asymmetric with respect to its orientation.[22] The anisotropic contributions can be described by expanding the potential in Legendre polynomials

$$V(z,\theta)=V_r(z)[1+\lambda_r P_2(\cos\theta)] + V_a(z)[1+\lambda_a P_2(\cos\theta)] , \quad (2.3)$$

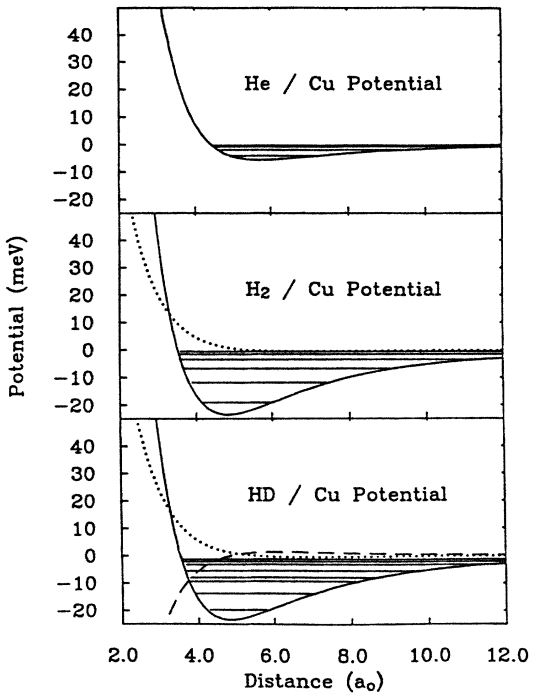

FIG. 1. The potentials used for calculating the inelastic-scattering probabilities. The top panel shows the helium-copper potential; the second panel, the H_2-copper potential, and the bottom panel, the HD-copper potential. The horizontal lines superimposed on each potential show the energy of each of the bound states of that potential (these are the bound states of the full orientationally-dependent potential); the lines, starting and stopping at the classical turning points for those energies, give some idea of the spatial extent of the bound-state wave functions. The two hydrogen potentials have been expanded in Legendre polynomials of the orientation of the molecular axis with respect to the surface normal; the solid curves are the $l=0$, angle averaged terms in the expansion, the dashed lines are the $l=1$ terms, and the dotted lines are the $l=2$ terms. Since the H_2 molecule has an axis of inversion symmetry, the $l=1$ term in the potential vanishes identically. The orientational dependence of the HD molecule is much stronger because its center of mass is offset from the centroid of the electron cloud.

where θ is the angle of orientation of the molecular axis with respect to the surface normal. Since H_2 has reflection symmetry only even terms enter the expansion in terms of Legendre polynomials, and since the orientational dependence is weak, only the second term contributes. The orientational dependence of the potential is shown in the second panel of Fig. 1.

Since the electronic structure of the HD and H_2 molecules are the same, the HD potential can be written in terms of the H_2 potential by

$$V_{HD}(z,\theta)=V_{H_2}(z+\delta\cos\theta,\theta) , \quad (2.4)$$

where δ is the offset of the center of mass with respect to the centroid of the electron cloud. This potential can be reexpanded in terms of Legendre polynomials and is plotted in the bottom panel of Fig. 1.

For comparison we also calculate scattering probabilities using a variety of Morse potentials. Morse potentials are potentials with a simple form requiring the minimum number of input parameters that reproduce the general shape of the surface potential

$$V_M(z)=D(e^{-2\alpha z}-2e^{-\alpha z}) . \quad (2.5)$$

The well depth D and the range parameter α are the two input parameters which for this calculation are chosen to match the well depth and range parameter of the exponential van der Waals potential. The Morse potential reproduces most of the features of the exponential van der Waals potential except the highest-lying bound states; the discrepancy is caused by the incorrect asymptotic behavior.

B. The interaction potential

While in general the interaction potential depends on the properties of each phonon in a complicated manner, in the local height approximation we assume that phonons shift the potential rigidly in the z direction by an amount $h(\mathbf{R},\{n_i\})$, where $\{n_i\}$ is the occupation of normal modes that differs from point to point in the surface plane. Then we expand the potential

$$V(z,\mathbf{R},\{n_i\})=V(z-h(\mathbf{R},\{n_i\})) , \quad (2.6)$$

in a Taylor series in the local height which, being typically much smaller than the characteristic length scales, allows us to truncate the expansion after the second term

$$V(z,\mathbf{R},\{n_i\})=V(z)-V'(z)h(\mathbf{R},\{n_i\}) . \quad (2.7)$$

The first term is the *static surface potential* and the second is a term linear in the phonon coordinates that will cause phonon transitions in the scattering process.

Many calculations in inelastic scattering assume that only the repulsive part of the potential couples to the phonons, i.e., replacing V' by V_r' in the second term of Eq. (2.7). We think a better approximation would be to

TABLE I. The parameters used in these calculations. For these calculations it is necessary to specify both the potential energy of helium (Ref. 26) or molecular hydrogen (Ref. 25) near a copper surface and the phonons of the copper surface in the elastic continuum model (Refs. 28 and 29).

		The potentials	
		He	H_2
Range parameter	α	$1.26a_0^{-1}$	$1.21a_0^{-1}$
Repulsive potential constant	V_0	12.0 eV	5.21 eV
van der Waals constant	C_{VW}	1.52 eV/a_0^3	4.83 eV/a_0^3
Mirror plane	z_{VW}	$0.462a_0$	$0.563a_0$
van der Waals cutoff	k_c	$1.0a_0^{-1}$	$0.4a_0^{-1}$
Well depth	D	5.66 meV	22.3 meV
Bound states	N_{BS}	5	7
		The phonons	
Longitudinal sound velocity	c_l	4.3×10^3 m/s	
Transverse sound velocity	c_t	2.2×10^3 m/s	
Rayleigh sound velocity	c_R	2.1×10^3 m/s	
Debye frequency cutoff	ω_D	30 meV	
Debye wave vector	Q_D	$0.907a_0^{-1}$	
Interaction potential wave vector cutoff	Q_c	$0.39a_0^{-1}$	

use the full potential. Typically the attractive part of the potential, far from the surface, is due to a large number of surface atoms so that when one atom moves it does not affect the potential, whereas the repulsive potential is local and dominated by the surface atoms closest to the scattering particle. In the region near the surface where the inelastic scattering takes place, however, breaking the potential into an attractive part and a repulsive part is somewhat artificial as the attractive part of the potential is also dominated by the closest surface atoms.

This choice of the interaction potential is shown in Fig. 2 for a simple model of the gas-surface potential. The potential is assumed to be a sum of a Morse potential from each layer in the solid. For this model the interaction potential is better approximated by the derivative of the full static surface potential rather than the derivative of the repulsive part of the same potential. This conclusion will depend on the details of the potential, but should be true for potentials close to this one; it is true for a sum of Lennard-Jones potentials. In Sec. III we will show that the choice of the interaction potential has a very strong effect on both the strength of the inelastic scattering and on the dependence of the inelastic scattering on the well depth of the potential.

We model the local height function as a sum over each lattice site of the displacement of that site times a Gaussian of the difference of the position in the plane of the surface between the particle and each lattice site

$$h(\mathbf{R},\{n_i\})=\sum_{i \text{ in surface}} u_{zi}\frac{\exp[-Q_c^2(\mathbf{R}-\mathbf{R}_i)^2/2]}{\sum_{j \text{ in surface}}\exp[-Q_c^2(\mathbf{R}-\mathbf{R}_j)^2/2]} . \tag{2.8}$$

The denominator in Eq. (2.8) normalizes the shift so that if the whole top surface layer makes a uniform shift, the origin of the potential will shift by the same amount. The cutoff $Q_c=0.39a_0^{-1}$ is primarily determined by the decay length of the surface density near the classical turning point and by the distance from the center of the displaced surface atom to the classical turning point and can be well approximated by considering just a single surface atom.[27] When we make the flat surface approximation, the sums over lattice sites become integrals and give

$$h(\mathbf{R},\{n_i\})=\int d^2R'\,u_z(\mathbf{R}')\times\exp[-Q_c^2(\mathbf{R}-\mathbf{R}')^2/2]\frac{Q_c^2}{(2\pi)} . \tag{2.9}$$

We use the values of Q_c that have been calculated for helium scattering from copper.[27]

C. The phonon spectra

The model we use is a semi-infinite isotropic elastic continuum model,[28,29] for which the appropriate density of states can be written down analytically. The primary defects of this model are that both the frequency and wave vector are unbounded and that the sound velocities are constants, independent of the wave vector. Besides its analytic solution the main advantage of this model is that it naturally includes the Rayleigh phonons which are localized to the surface and are the lowest frequency phonon modes at each wave vector. The Rayleigh phonon

modes are responsible for roughly one-half of the mean-square displacement of the surface. The choices for the phonon parameters are given in Table I.

Figure 3 shows both the mean-square displacement of the surface as a function of temperature and the effect of the high wave vector cutoff, discussed in Eq. (2.8), on the mean-square effective height of the surface. The value of the cutoff used in this paper drastically reduces the mean-square effective height of the surface compared to the mean-square displacement of the surface. This reduction decreases the inelastic scattering from what it would be if the unphysical coupling to high wave vector phonon were retained.

Figure 4 shows the weighted density of phonon states as a function of the energy change in the motion normal to the surface due to each phonon

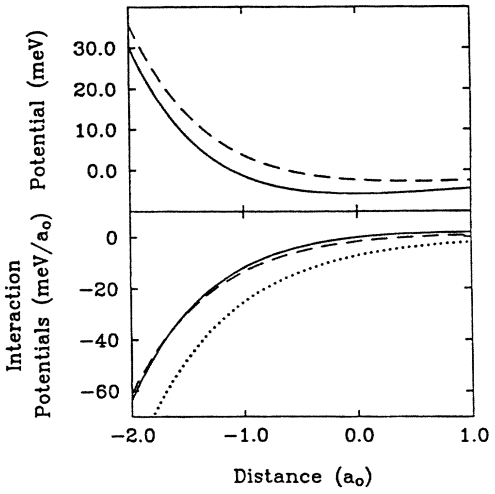

FIG. 2. A Morse potential model for the interaction potential. To study possible forms of the interaction potential a Morse potential form of the gas-surface potential can be constructed from a Morse potential contribution from each layer in the solid. The top panel shows the resulting static surface potential (solid line) and the contribution to this potential from the top layer of the surface (dashed line). The difference between these two potentials shows that a large part of the attractive well is due to the subsurface layers even for a potential as short ranged as a Morse potential. The bottom panel shows the derivative of the static surface potential (solid line), the derivative of the contribution from the top layer (dashed line), and the derivative of the repulsive part of the static surface potential (dotted line). The interaction potential for phonon modes in which the top surface layer rigidly shifts normal to the surface is given (in the low-amplitude limit) by the derivative of the potential due to the top layer of the solid. This figure shows that this interaction potential is much better approximated by the derivative of the full static surface potential than by the derivative of the repulsive part of the static surface potential even though the subsurface layers make a large contribution to the attractive region of the potential. The static surface potential is a better approximation because the attractive part of the potential is more strongly dominated by the top layer contribution the closer the particle is to the surface.

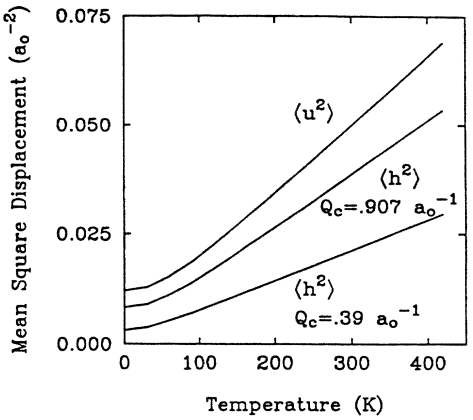

FIG. 3. The mean-square displacement of the surface. This figure shows as a function of surface temperature the mean-square displacement of the surface (top curve), and the mean-square displacement of the effective height of the surface for two choices of the cutoff wave vector. This cutoff is contained in the interaction potential as a factor that reduces the contribution to inelastic scattering of high-parallel wave vector phonons. At temperatures high compared to the Debye temperature all three curves are roughly proportional to the surface temperature and go to a finite value at zero temperature due to the zero-point motion of the surface. The lowest curve is for the cutoff used in these calculations, and the middle curve is for the cutoff equal to the surface reciprocal lattice vector appropriate to these calculations.

$$C(\Delta E_z)=\frac{1}{N}\sum_{\lambda,\sigma} n_{\lambda\sigma}\,|M_\lambda|^2 \times(2\pi)\delta\left[\sigma\omega_\lambda-\left[\Delta E_z-\frac{(\mathbf{K}_i-\sigma\mathbf{Q}_\lambda)^2}{2m}+\frac{K_i^2}{2m}\right]\right]. \quad (2.10)$$

M_λ is defined in Eq. (5.13) of I and is a measure of the amplitude of the phonon projected onto the surface layer, λ indexes the normal modes of the semi-infinite lattice, and $\sigma=\pm$ indexes creation and destruction events. The integral of this density times the matrix element of the particle-scattering states gives the inelastic-scattering probability. Since the high parallel wave vector cutoff has a larger effect on high-energy phonons than it does on low-energy phonons, the inclusion of the cutoff reduces the probability for high-energy transfer inelastic-scattering events. It also reduces the asymmetry between the energy loss and energy gain inelastic-scattering probabilities.

III. RESULTS

This section details our calculations of elastic- and inelastic-scattering probabilities. In Sec. III A are results for helium scattering from copper with the emphasis on both the effect of inelastic scattering on elastic scattering and the effect of the shape of the surface potential on the various scattering probabilities. Section III B, which gives the results for molecular-hydrogen scattering,

presents the interplay of inelastic scattering and rotationally inelastic scattering.

A. Helium scattering

We investigate five models for the elastic-scattering probability, three related to the distorted-wave Born approximation, and two related to the descriptions of diffraction intensities in x-ray and neutron scattering. Of the first three methods, two are based on a one-phonon approximation and are described in I, and the last is an attempt to extend these approximations into the multiphonon regime (this is discussed later in this section). Evidence that helium scattering can be described in terms of one-phonon creation and destruction events comes from the observation of such events by time-of-flight helium scattering experiments.[30,31] The first of the last two methods (both discussed in this section) applies the Debye-Waller expression for the temperature dependence of neutron-scattering intensities to surface-scattering problems, and the second attempts approximately to include the effect of the attractive potential. These methods are compared in Fig. 5, which shows the scattering probability as a function of surface temperature.

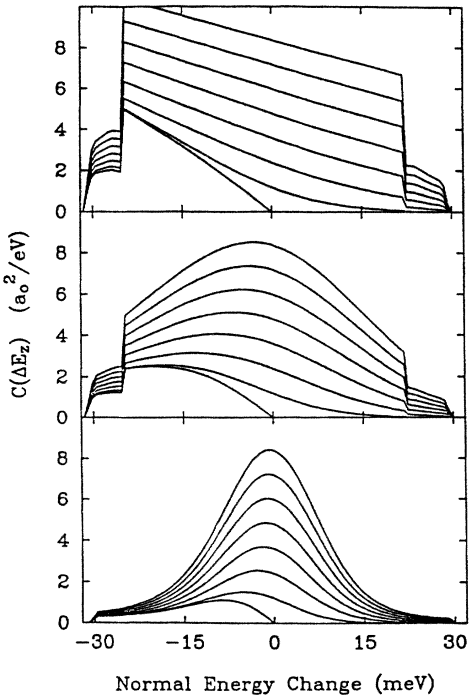

FIG. 4. The dependence of the phonon density of states on the change in energy in the inelastic-scattering process for several surface temperatures. These three panels show for surface temperatures ranging from 0 to 420 K in steps of 60 K, the density of phonons (weighted by their amplitude projected on the surface layer) as a function of the change in the normal energy of the scattering particle. Each of the three panels corresponds to one of the weightings of the density by the high-parallel wave vector cutoff that are discussed in Fig. 3, i.e., the top panel shows the energy density of all phonons, and the two lower panels show the energy density of the phonons reduced by the large-wave vector cutoff in the interaction potential for the same two values of the cutoff wave vector (as in Fig. 3). The effect of the large-wave vector cutoff is to reduce the weight of phonons contributing to large normal energy changes without strongly affecting the low-energy transfers, because low-frequency phonons necessarily have low-parallel wave vectors. The steps in these curves, which are most pronounced in the top panel are due to the Debye parallel wave vector cutoff of the Rayleigh phonons.

We start with the distorted-wave Born approximation. The first term in the Born series yields the scattering probability from the static surface which is unity for an uncorrugated system with no translational-rotational coupling. The correction due to the inelastic scattering to this first term is equal to the negative of the total first-order inelastic-scattering probability, i.e., the lowest-order expression for the effect of inelastic scattering on elastic scattering is just one minus the total first-order inelastic-scattering probability calculated in the distorted-wave Born approximation (DWBA)

$$P_{\rm el}^{\rm DWBA}=1-P_{\rm inel}^{\rm DWBA}\ . \tag{3.1}$$

This result is valid only when the inelastic-scattering probability is small compared to unity—a limit which is seldom attained in experiments. When the distorted-wave Born approximation for the inelastic-scattering probability becomes greater than one (which is allowable in this approximation) Eq. (3.1) produces a negative elastic-scattering probability.

The second method considered is also a one-phonon approximation, the self-consistent one-phonon approximation developed in I. Essentially it makes the one-phonon approximation in the self-energy of the scattering particle rather than in the scattering probability. Even though this approximation constrains the elastic scattering to lie between zero and one, it is nonetheless a one-phonon approximation and does not have a significantly larger range of validity than the Born series. It is especially useful for calculating the temperature dependence of diffraction and rotational diffraction intensities near selective adsorption resonances.

To extend these distorted-wave Born approximation methods into the multiphonon regime we invoke the exponentiated inelastic-scattering model. As its name suggests it involves exponentiating the first-order inelastic-scattering probability to predict the elastic scattering

$$P_{\rm el}^{\rm EI}=\exp(-P_{\rm inel}^{\rm DWBA})\ . \tag{3.2}$$

In the weak-scattering limit the expanded exponential is identical to the distorted-wave Born approximation result, and the probability is bounded between zero and one. Even though this method is the best available extension of the one-phonon results to the multiphonon regime, it must be regarded as *ad hoc*. Two possible defenses of this approximation might be (1) that it is the result of a cumulant expansion[4] and (2) that the probability for a n-phonon-change scattering event might be a Poisson distribution.[32] Unfortunately, (1) the other terms in the cumulant expansion have not been checked to see how important they are, and (2) multiphonon terms, which have only been calculated for approximate potentials that have a form that simplifies the calcula-

tion,[3,33–35] give results that are incompatible in detail with a Poisson distribution.

Figure 5, a Debye-Waller plot, shows the temperature dependence of the elastic-scattering probability. It is called a Debye-Waller plot because similar plots of neutron-scattering intensities give straight lines for temperatures larger than the Debye temperature of the surface. The right-hand scale displays the negative of the natural logarithm of the elastic-scattering probability; for the exponentiated inelastic-scattering model this is equal to the distorted-wave Born approximation result for the inelastic-scattering problem and hence can be used to gauge when the scattering is in the one-phonon regime and when it is in the multiphonon regime.

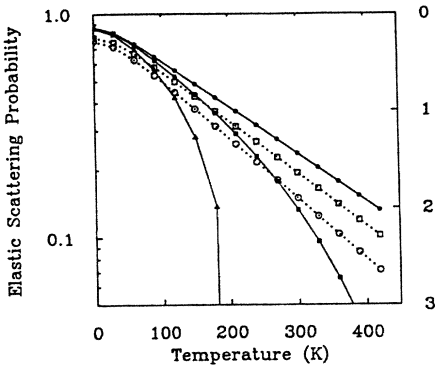

FIG. 5. A comparison of different calculations of elastic-scattering probabilities as a function of temperature. The results of three calculations based on the distorted-wave Born approximation (solid curves) and two based on a Debye-Waller approach (dotted curves) are compared for calculations of the elastic-scattering probability for helium scattering from copper at normal incidence. The three distorted-wave based methods are (1) the second-order distorted-wave Born approximation (solid triangles), (2) the self-consistent one-phonon approximation (solid squares), and (3) the exponentiated inelastic-scattering model (solid circles). The axis on the left-hand side of the figure gives the elastic-scattering probability on a logarithmic scale, and the axis on the right-hand side gives the natural logarithm of the elastic-scattering probability. For the exponentiated inelastic-scattering model the (negative) natural logarithm of the elastic-scattering probability is just the distorted-wave Born approximation result for the total first-order inelastic-scattering probability. The total inelastic scattering can be used to gauge the temperatures for which the one-phonon approximation is valid because the first-order inelastic scattering probability should be small compared to one; this condition is not satisfied for most of the temperatures on this plot. The second-order distorted-wave Born approximation becomes zero when the first-order Born approximation becomes one; this behavior leads to a divergence in this scattering probability seen in this figure at 220 K. The self-consistent one-phonon result is bounded between zero and one so that there are no divergences but the curvature as a function of temperature is affected by the breakdown of the one-phonon approximation. In the high-temperature limit the distorted-wave Born result for the inelastic scattering is proportional to the temperature; in this limit the exponentiated inelastic-scattering model gives results that are linear on this plot. The other two results, both of which are proportional to the temperature in the high-temperature limit are the Debye-Waller factor (open squares) and the Beeby-corrected Debye-Waller factor (open circle). Both of these quantities are calculated using the mean-square effective height of the surface rather than the mean-square displacement because the former quantity is used in the distorted-wave methods, this choice increases the log of the scattering probability by a factor of roughly 2.5.

This plot shows that all three methods agree well in the one-phonon regime where the inelastic scattering is small compared to one, but disagree in the multiphonon regime. When the inelastic-scattering probability exceeds unity, the distorted-wave Born results diverges on this type of plot. In addition to a physical curvature in each curve at low temperatures due to the zero-point motion of the surface, there is unphysical curvature at high temperatures in the distorted-wave Born series results due to the divergence caused by the increasing inelastic scattering outside the one-phonon regime. Even though the elastic-scattering probability in the self-consistent one-phonon approximation is bounded between zero and one, there is a downward curvature outside the one-phonon regime (where the distorted-wave Born approximation results are not small compared to one, which occurs at high temperatures in this plot). This is not to say that straight-line behavior is expected, just that the observed deviations in these curves are unphysical and hence meaningless. This curvature is necessarily absent from the exponentiated inelastic-scattering model because the distorted-wave Born approximation inelastic-scattering probability is proportional to the temperature for temperatures larger than the surface Debye temperature. Since none of these models are valid in the multiphonon regime, none can reliably predict in that regime that the logarithm of the elastic-scattering probability should be proportional to the temperature in this limit or that there should be less or more elastic scattering.

The other two methods shown in these two figures are related to the Debye-Waller factor. The temperature dependence of the specular-scattering probability (specular scattering is elastic scattering without diffraction, for a flat surface specular and elastic scattering are the same) is

$$P_{\rm el}^{\rm DW} = \exp[-8mE_z\langle u_z(\mathbf{R})^2\rangle_{th}] , \tag{3.3}$$

where E_z is the energy in the motion normal to the surface. For diffraction there are also contributions from the motion of the particle and the phonons in the plane of the surface, but these are less important, both in general and especially for the flat surfaces we are considering. There is no reason to expect that this expression, which is derived for neutron scattering, should describe surface scattering. In addition to the complications due to the strength of the scattering, i.e., weak for neutrons and strong for helium, the potential for an atom scattering from a surface is much different than it is for neutron scattering from a solid. In particular the potential is soft as opposed to delta-function-like, there is an attractive part to the potential, and the potential cannot be described by a sum of pair potentials.

This result, Eq. (3.3), can be modified in several ways to approximately include some of the physics that is

different in surface-scattering situations. One way, illustrated in Fig. 5, is to use the mean-square effective height of the surface rather than the mean-square displacement

$$P_{\rm el}^{\rm DW} = \exp[-8mE_z\langle h(\mathbf{R})^2\rangle_{th}] \ . \tag{3.4}$$

Since the mean-square displacement is more than twice as large as the mean-square effective height, if we were to use the former (3.3) in place of the latter (3.4), the elastic-scattering probability would be much smaller and further from the perturbation-theory-based results in the weak-inelastic-scattering limit.

Surprisingly it is possible to account for most of the changes in scattering probabilities for systems with different attractive potentials by shifting the incident normal energy by the change in the well depth. Use of this shift in the Debye-Waller factor leads to

$$P_{\rm el}^{\rm BCDW} = \exp[-8m(E_z+D)\langle h(\mathbf{R})^2\rangle_{th}] \ , \tag{3.5}$$

where D is the well depth. Known as the Beeby-corrected Debye-Waller factor,[36] in Fig. 5 it moves (cf. Fig. 5) the elastic-scattering probability even further from the perturbation-based results. This increased deviation could be compensated for by including the effects of the softness of the surface potential because that correction would increase the elastic-scattering probability from the Debye-Waller result. In Sec. III A 1 we study the effect of a steeper potential on the elastic-scattering probability. We find that in the hard-wall limit the elastic-scattering probability is very close to the Beeby-corrected Debye-Waller result implying that the differences are due to the softness of the potential. Unfortunately we know of no simple way to account for the softness of the potential in a Debye-Waller-like analysis; a correction that would have to depend not only on the range parameter of the potential but also on the well depth and on the scattering energy.

Figure 6 compares elastic-scattering probabilities, calculated using the exponentiated inelastic-scattering model, with experimentally measured ones.[37,38] The agreement is surprisingly good for a calculation with no adjustable parameters, although it is better for the 63-meV results than it is for the 21-meV results which are closer to the one-phonon regime in which this calculation should be more reliable. The experimental data cover a larger range of temperatures than that shown here. At higher temperatures the inelastic scattering is so strong that a one-phonon-based theory really should not apply; the elastic scattering departs from linearity on a Debye-Waller plot. Possible explanations are either that this departure is a natural consequence of the perturbative expansion[2] or that it is due to anharmonic behavior of the phonons at the surface.[39] Similar effects have been seen for helium scattering from nickel.[39] We view the latter explanation as more likely both because it should be present in some degree and because the first explanation is based on calculations outside their range of validity.

The assumptions about the potential that have the largest effect on the scattering probability are (1) the choice of the form and values for the dependence of the interaction potential on the phonon parallel wave vector, (2) the range parameter of the repulsive potential, and (3) the choice of using the derivative of the full potential or of the repulsive potential in the interaction potential. The effect of the first assumption is illustrated in Fig. 3 which compares the mean-square displacement of the surface with the mean-square effective height of the surface. The inelastic-scattering probability is roughly proportional to the mean-square effective height; if the parallel wave vector cutoff were not included in the interaction potential, the inelastic scattering would be approximately twice as large. This difference highlights the difficulty in extracting information about the scattering system from the experimental temperature dependence; here the mean-square effective height that would be extracted from these calculated curves in a Debye-Waller analysis is not simply related to the mean-square displacement of the surface atoms.

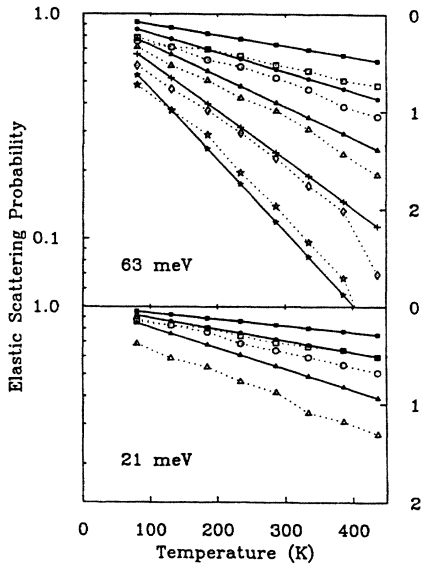

FIG. 6. Comparison of calculated with experimental elastic-scattering probabilities. The two panels show experimentally measured (Ref. 38) (dotted curves and open symbols) and theoretically calculated (solid curves and symbols) elastic-scattering probabilities as a function of surface temperature for two incident energies, 63 meV in the top panel and 21 meV in the bottom, and several incident angles 71.6° (squares), 6.17° (circles), 51.9° (triangles), 39.0° (diamonds and crosses), and 19.0° (stars) in the upper panel and 73.5° (squares), 55.5° (circles), and 3.18° (triangles) in the lower panel. The agreement is surprisingly good for a comparison with no adjustable parameters and may be fortuitous given the uncertainty in some of the approximations made in this model. The probabilities have been calculated using the exponentiated inelastic-scattering method (discussed in Sec. III A) with additional assumptions about the form of the potential which includes the flat-surface approximation (see I), the isotropic elastic continuum model for the phonon spectrum (Sec. II C), and the form of the interaction potential (Sec. II B). Using the derivative of the repulsive potential rather than the full potential in the interaction potential will increase the inelastic scattering, or the exponent in the exponentiated inelastic-scattering model, by roughly a factor of 4. Ignoring the wave vector cutoff in the interaction potential will increase the inelastic-scattering probability by slightly more than a factor of 2.

1. Dependence on potential parameters

The sensitivity of the elastic-scattering probability to the choice of the potential can be tested using a Morse potential, which allows easy variation of the potential parameters. Calculations[3,2] using a one-dimensional model and the distorted-wave Born series have found results similar to these calculations. We use the exponentiated inelastic-scattering model because it is the simplest and because the behavior should not differ from the other two perturbation-based approaches in the regime where the three can be trusted. Figure 7 shows the elastic-scattering probability for the exponential van der Waals potential and a Morse potential chosen to have the same well depth and the same range parameter for the repulsive part of the potential.

We attribute the slight difference between the two results to the difference between the attractive potentials in the region near the classical turning point. As we show in Sec. III B, the inelastic scattering primarily takes place near the classical turning point and not in the region where the potential is dominated by the attractive potential. At the classical turning point this Morse potential is steeper than the exponential van der Waals potential so the inelastic scattering is stronger, and hence the elastic scattering is weaker for the Morse potential than it is for the other. That a steeper potential gives weaker elastic scattering is borne out by studying the elastic-scattering probability as a function of the range parameter.

Figure 7 also shows the elastic-scattering probability for several other Morse potentials in which the range parameter varies by a factor of 16. As expected a steeper potential produces stronger inelastic scattering, although the variation is much more dramatic as the range parameter is decreased. The results for the two steepest potentials lie on top of each other indicating that the potential has reached a hard-wall limit. The differences between the results for the physical potential and the results for the potentials in the hard-wall limit are very close to the differences between the physical potential and the Beeby-corrected Debye-Waller factor results in Fig. 6. For these systems, helium and molecular hydrogen on copper, the potential is close to but not in the hard-wall limit.

In the previous section we mentioned that the effect of the attractive potential can be accounted for to a large extent by adding the well depth to the energy in the motion normal to the surface; this is examined in Fig. 8 by varying the well depth of the Morse potential by a factor of 8. Adding the well depth does not completely correct for the effects of the attractive potential because the Morse and exponential van der Waals potentials that have the same well depths, but different forms of the attractive potential do not have identical scattering probabilities (as seen in Fig. 7). The difference is due to the slope at the classical turning point depending on the form of the attractive potential even for potentials that give the same well depth. If the idea behind the Beeby correction is correct, the curves in this figure should be shifted with respect to each other along the energy axis by an amount equal to the difference between the well depths. Using the inset at the top of the figure as a guide, this is seen to be correct for this choice of range parameter and these various well depths.

The Beeby correction would be exact (i) if the part of the potential further from the surface than the well minimum were both decoupled from the phonons and sufficiently slowly varying and (ii) if the entire potential inside the well minimum, i.e., both the attractive and repulsive contributions were coupled to the phonons. The results in Fig. 8 show that these conditions are well satisfied for this potential. On the other hand, if only the repulsive part of the potential is coupled to the phonons,[2,3] these conditions are not satisfied, and the Beeby correction is not a good approximation. The two types of coupling disagree by roughly a factor of 2 in the amount of inelastic scattering predicted.

By comparing He and D_2 scattering from several flat surfaces, it should be possible to distinguish between models for the interaction potential because, except for the presence of weak rotationally mediated selective adsorption resonances, the most important difference between the two systems is the strength of the attractive potential. The surfaces should be flat because the increased attraction for the deuterium molecular can also increase the effective corrugation that the molecule experiences.

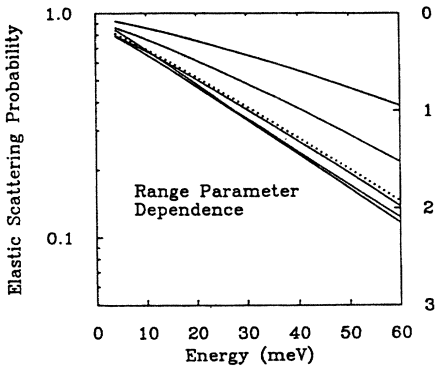

FIG. 7. The range parameter dependence of the elastic-scattering probability. The inelastic-scattering probability in the distorted-wave Born approximation (the right-hand scale) and the elastic-scattering probability in the exponentiated inelastic-scattering model (same curves, but left-hand scale) are shown as a function of incident energy for different models of the potential. The dotted line is calculated using the exponential van der Waals potential used in the previous figures, and the solid line closest to it is calculated using the Morse potential with the same well depth and range parameter in the repulsive part of the exponential van der Waals potential. This and Fig. 8 show how the inelastic scattering changes as a function of the potential that is used to calculate it. Here, the range parameter of the Morse potential is varied in the series $\alpha=\alpha_0/4$, $\alpha_0/2$, $\alpha_0, 2\alpha_0$, $4\alpha_0$, where $\alpha_0=0.63a_0^{-1}$, giving the curves from the uppermost to the lowest, respectively. The well depth for these potentials is $D_0=5.656$ meV. The curves for the two steepest potentials $\alpha=2\alpha_0$ and $\alpha=4\alpha_0$ but not that for $\alpha=\alpha_0$ are coincident to within the accuracy of the calculation indicating that while the first two potentials are both in the hard-wall limit the latter is not. The difference between the results for the hard-wall potential and the physical potential account for much of the differences between the Beeby-corrected Debye-Waller factor results and the results for the physical potential.

We also find that over the range of potentials we have investigated inelastic scattering is proportional to the mass as is predicted by the Debye-Waller and related treatments. The distorted-wave Born approximation integrated over all final momenta depends on the mass through an overall factor of mass and the mass dependence of the wave functions. The mass dependence of the incident wave vector at constant incident energy is canceled by a similar factor from the integration over the final states. That the inelastic-scattering probability scales with the mass implies that the matrix element of the scattering states is only very weakly dependent on the mass.

We summarize the dependencies we have found. (1) The potentials we use for helium and hydrogen scattering are almost but not quite in the hard-wall limit with respect to the variation of the range parameter. (2) For the model of the interaction potential we are using, the effect of the attractive potential can be accounted for by adding the well depth to the incident energy in the motion normal to the surface (but not if we were to use the repulsive potential inelastic coupling). (3) The inelastic scattering, which is the exponent in the exponentiated inelastic-scattering model, is proportional to the mass of the scattering particle. Previously, in Sec. II C, we showed that (4) the inelastic scattering is roughly proportional to the effective mean-square effective height based on the form of the phonon-wave vector dependence of the interaction potential.

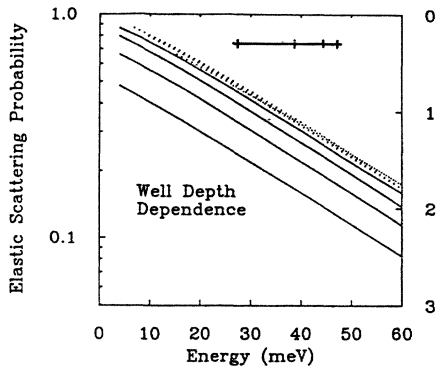

FIG. 8. The well depth dependence of the elastic-scattering probability. Similarly to Fig. 7, the elastic-scattering probability calculated using the exponentiated inelastic-scattering model is shown as a function of energy for a variety of potential well depths. For the curves from the top to bottom the well depths are $D=D_0/2$, $D=D_0$, $D=2D_0$, and $D=4D_0$, where the physical well depth is $D_0=5.656$ meV. The ticks on the inset in the top right-hand corner give the separation of the energies of the potential wells used in these calculations; Beeby-corrected Debye-Waller calculations give elastic-scattering probability curves separated by these amounts. Surprisingly this exponentiated inelastic-scattering model gives the same result indicating that the potential beyond the well minimum only contributes to the dynamics by speeding up the incident atom. The dotted curves are each of the calculated curves shifted horizonally by the well depth of the potential that was used to calculate them. This result does not occur if only the repulsive part of the potential is included in the interaction potential.

2. *Optical potentials*

It would be desirable to develop an approximation scheme that could be used to calculate elastic-scattering probabilities more simply than is done in this calculation. Above we concluded that Debye-Waller factors can be used with phenomenological fitting factors but need drastic modification to be used to predict scattering probabilities. Another possible approach is to use an optical potential, a potential with an imaginary part that causes flux to be absorbed from the incident wave function. We have not been able to find a model that can reproduce the desired features; to illustrate the difficulty we have calculated the self-energy for the self-consistent one-phonon approximation [see Eq. (4.12) of I]. The self-energy is equivalent to a nonlocal energy-dependent optical potential because the zero-phonon-change amplitude discussed in I satisfies

$$(H_{\rm part}-E_{\mathbf{k}}-i\eta)\psi_{0\rm ph}^{(+)}(\mathbf{r},\mathbf{k}) = \int d^3r'\,\Sigma(\mathbf{r},\mathbf{r}',E_{\mathbf{k}})\psi_{0\rm ph}^{(+)}(\mathbf{r},\mathbf{k})\ , \quad (3.6)$$

where Σ is the self-energy calculated in the one-phonon approximation. Using the assumptions for the form of the interaction potential discussed in I, the self-energy reduces to

$$\Sigma(z,z',E_z)=\int \frac{d(\Delta E_z)}{2\pi} V'(z)G_1^r(z,z',E_z-\Delta E_z-i\eta) \times C(\Delta E_z)V'(z')\ . \quad (3.7)$$

The Green's function can be calculated for small but finite value of the imaginary piece η by using its spectral form.

Figure 9 shows the imaginary part of the self-energy for three different energies as a function of the two spatial arguments for a surface temperature of 240 K. The main point of this figure is that it is very difficult to approximate this function in any manner that retains the important physics. The difficulty arises because this self-energy is strongly energy dependent, nonlocal, and nonseparable as well as being temperature dependent. The energy dependence of the elastic-scattering probability results from the energy dependence not only in the incident scattering state, but also from energy dependence of the final scattering states near the incident energy. This dependence on the final states complicates any optical potential treatment because the strength of the optical potential depends on the incident energy. Any local optical potential[40] would have to be regarded as *ad hoc*.

The nonlocal and nonseparable aspects of an optical potential will drastically slow any numerical calculation. If the self-energy were approximately local, i.e., proportional to a δ function of the difference of the two spatial arguments, it would be possible to treat the optical potential as though it only had one spatial argument, which would allow calculating scattering probabilities in a way that would not be much more complicated than the calculation for a static surface. On the other hand, if the self-energy dependence were separable, the calculation of the scattering probabilities would involve an extra spatial

integration over the second spatial argument, but that integration could be done independently of the other spatial argument allowing a simple self-consistent solution of just a single differential equation. The temperature dependence of the self-energy would be well approximated as proportional to the mean-square effective height of the surface.

B. Molecular-hydrogen scattering

Molecular-hydrogen scattering differs from helium scattering because (1) the mass is different (except for D_2), (2) the potential well is deeper because the attractive potential is stronger, and (3) the molecule has rotational degrees of freedom. The effects of changing the mass and the well depth are among the topics discussed in Sec. III A. The rotational degrees of freedom affect molecular-hydrogen scattering in two ways: (1) the molecule can make rotational transitions, both real transitions and virtual rotational transitions into bound states of the surface potential, and (2) the potential of the molecule depends on its rotational state (even if no rotational transitions occur). For H_2 and D_2 the effects of the rotational degrees of freedom are much less important than they are for the much more asymmetric HD molecule.

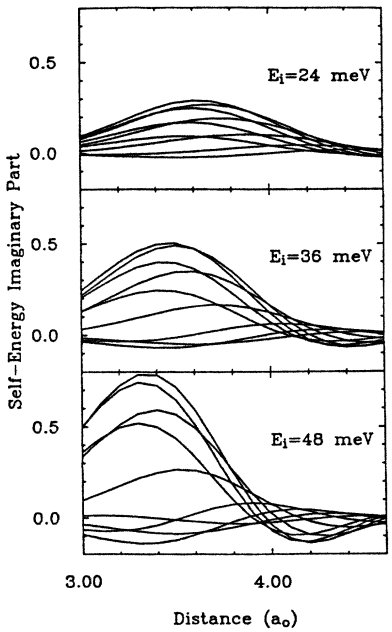

FIG. 9. The self-energy for helium scattering from copper in the one-phonon approximation. The imaginary part of the nonlocal self-energy [see Eq. (3.7)] is plotted as a function of the first spatial argument with the second spatial argument taking the values $z'=3.0,3.2,\ldots,4.6a_0$ for three different energies (given in each panel). The static surface potential for helium scattering that is used in these plots is shown in Fig. 1, and the phonon density as a function of energy is shown in the bottom panel of Fig. 4 as the 240 K curve. To associate each curve in a panel with its second spatial argument, find the curves for which the first peak (moving from left to right) occurs at the same position; the curve with the lowest peak height has the lowest value of the spatial argument. The first peak in the optical potential is near the classical turning point ($z=3.6a_0$ for $E_i=24$ meV, $z=3.45a_0$ for $E_i=36$ meV, and $z=3.3a_0$ for $E_i=48$ meV). This peak height increases as the second spatial argument increases until it reaches a maximum. Then as the second argument increases further the peak shifts to the right and decreases, reaching the rightmost part of the panel for the last included value of the second spatial argument. The self-energy goes to zero for large values of either spatial argument because the interaction potential vanishes and goes to zero for small (and negative) values of either spatial argument, because there are no inelastic wave functions with energies near the incident energy that penetrate into the surface.

1. *Selective adsorption resonances*

Although the rotational effects are more prominent for HD scattering they can still be seen for H_2 and D_2 in Fig. 10 which shows the inelastic-scattering probability calculated in the distorted-wave Born approximation for different incident angular momentum states. Experimentally[41-44] hydrogen diffraction, rotationally inelastic scattering, and selective adsorption resonances have been observed. However, the resonances are too weak to measure the interaction between selective adsorption and inelastic scattering.

The large peaks in Fig. 10 are due to the selective adsorption resonance enhancement of the inelastic scattering. A rotationally mediated selective adsorption resonance occurs when a molecule makes a virtual rotational transition into a bound state of the gas-surface potential and spends a long time in this rotationally excited state before it leaves the surface. Typically selective adsorption resonances are seen in a scattering experiment through diffraction (or rotational diffraction) intensities; at the resonances there are large rearrangements of the scattering intensities between various elastic- and rotationally inelastic-scattering channels (allowed zero-phonon-change final states). For low-incident energies in the systems studied here specular scattering is the only possible zero-phonon-change final state, i.e., no rotational transitions can occur and no rearrangement can take place. However, selective adsorption resonances still have experimental consequences, because they enhance inelastic scattering which in turn changes the elastic-scattering probability. Resonantly enhanced inelastic scattering has been seen using time-of-flight measurements for helium scattering from corrugated surfaces.[45-47]

Since the particle spends a long time in the region of the potential minimum the probability for inelastic scattering is increased giving the peaks seen in Fig. 10. For these symmetric hydrogen molecules the translational-rotational coupling is very weak so that the resonances are narrow, i.e., once a molecule makes a transition into a rotationally trapped state it remains there for a long time before it makes a transition out of the trapped state (ignoring inelastic scattering).

At this point it is useful to define several terms used in this discussion of selective adsorption resonances, particularly with respect to the widths of the resonances as a function of energy (all widths refer to functions of energy in this section). The term static surface refers to the surface with all of the lattice displacements fixed to zero and

should not be confused with a zero-temperature surface for which the lattice atoms move with their zero-point motion. If we hypothetically scatter molecules from a static surface there is no inelastic scattering, and the selective adsorption resonances have a width that is determined by the translational-rotational coupling; we call this width the elastic width and its inverse the elastic lifetime

$$\Gamma_{\rm el}=\tau_{\rm el}^{-1} . \tag{3.8}$$

For particles that scatter from a surface that is free to move, even if it is zero temperature, the width of the selective adsorption resonances increases due to the inelastic scattering. The width of a resonance is given by the sum of the elastic width and the inelastic width

$$\Gamma=\Gamma_{\rm el}+\Gamma_{\rm inel}=\frac{1}{\tau}=\frac{1}{\tau_{\rm el}}+\frac{1}{\tau_{\rm inel}} . \tag{3.9}$$

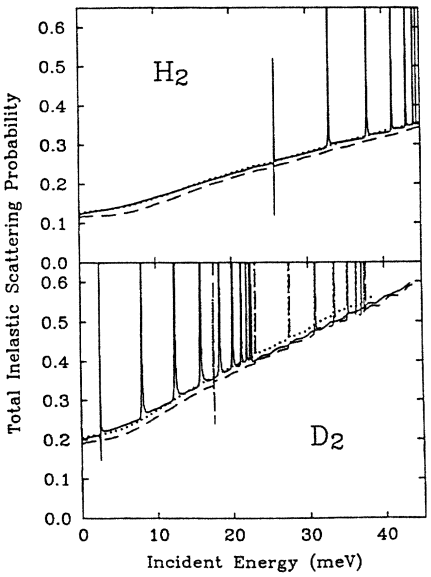

FIG. 10. Molecular-hydrogen inelastic-scattering probabilities. The top panel (H_2) and the bottom panel (D_2) show the distorted-wave Born approximation results for the inelastic-scattering probability for molecular-hydrogen scattering from a zero-temperature copper surface. The three curves—solid ($l=0$, $m=0$), dashed ($l=1$, $m=0$), and dotted ($l=1$, $m=1$)—are for different rotational states of the incident molecule. These three states are not coupled by the surface potential because the flat surface conserves the azimuthal quantum number, and there is no nuclear spin coupling to convert ortho (odd l H_2 and even l D_2) to para (even l H_2 and odd l D_2) or vice versa. For the low incident energies the scattering is in the one-phonon regime except at selective adsorption resonances which are the sharp narrow peaks in the inelastic-scattering probability. The inelastic scattering is so strongly enhanced at resonances to the point where it is well outside the one-phonon regime. The difference between the curves in each panel are due to (1) the different rotational energy splittings for the odd and even angular momentum species leading to different selective adsorption resonance energies and (2) the different spherical harmonic matrix elements of the potentials that are important for each species. The differences between H_2 and D_2 are due to the difference in the mass leading to (1) stronger inelastic scattering for D_2, (2) lower rotational energy splitting so that the resonances occurs at lower energies, and (3) more and more closely spaced bound states for D_2.

In the distorted-wave Born approximation the resonances are not broadened by the inelastic scattering, so the width of the resonant enhancement of the inelastic scattering is given by the elastic-scattering width. The self-consistent one-phonon approximation allows the inelastic scattering to affect the elastic scattering in a way that allows the resonances to broaden inelastically. Most of the resonances we discuss have inelastic widths that are greater than their elastic widths when calculated in the self-consistent one-phonon approximation.

The narrow H_2 and D_2 resonances produce enhancements of the inelastic-scattering probability that are so large that the distorted-wave Born approximation used to calculate the scattering probabilities is not valid. Unfortunately calculations using the self-consistent one-phonon approximation are difficult because the peak heights are so large that an iterative solution does not converge even when the background values of the inelastic-scattering probability are in the one-phonon regime. Nonetheless the results of the self-consistent calculation applied to HD scattering can be used to qualitatively understand what happens to H_2 and D_2 scattering near selective adsorption resonances when inelastic scattering is important. Both HD resonances and H_2 and D_2 resonances for which the inelastic width is much larger than the elastic width should behave similarly to each other because the processes that contribute to the elastic width are similar.

The resonant enhancements, although extremely large, are narrow enough that their contribution to the inelastic scattering is comparable to the background when both the resonant contribution and the background are integrated over a typical experimental resolution of 0.5 meV. For instance, the H_2 resonance near 33 meV has a width of about 4×10^{-3} meV and a weight integrated over energy of 0.7 meV while the background at that energy integrated over 0.5 meV has a value of 0.2 meV. If inelastic scattering did not affect the resonance widths the resonances would show up as suppressions of the elastic-scattering probability. However the peak value of the inelastic scattering at the 33 meV resonance is 56 which is an unacceptable value for a scattering *probability*. Since the peaks are so large, they broaden considerably to the point where the widths of the peaks are dominated by the inelastic lifetime as opposed to the elastic lifetime that determines the widths of the peaks as seen in Fig. 10. The broadened peaks will have a much smaller effect compared to the background inelastic scattering as is seen below in the temperature dependence of the HD resonances. The inelastic lifetimes of the HD selective adsorption resonances which should be comparable to the inelastic lifetimes of the H_2 and D_2 resonances are much shorter than the elastic lifetimes of the H_2 and D_2 resonances.

The resonances are different for H_2 and D_2 because the mass and hence the moment of inertia are larger for the latter. The larger D_2 mass yields more bound states in

the gas-surface potential, and further the bound states are closer together in a given energy range. The mass also increases the background value of the inelastic-scattering probability by roughly a factor of 2 as was discussed in Sec. III A 1, and hence the height of the resonances is also increased by a factor of 2 over what it would be if the other aspects of the resonance were unaffected by the difference in the mass. Since the moment of inertia is also larger by a factor of 2 for D_2 compared to H_2 the rotational energy splitting is smaller and the resonances occur at lower energies than they do for H_2.

The differences between the inelastic-scattering probabilities for different incident angular momentum states arise from the differences in the spherical harmonic matrix elements of the potential. [See Eq. (5.6) of I.] The inelastic-scattering probability is determined (for these systems with weak rotational coupling) by the diagonal matrix element of the potential with the incident rotational state. The energies of the selective adsorption resonances, on the other hand, are determined by the diagonal matrix element with the rotationally excited states.

These differences in the inelastic-scattering probabilities lead naturally to the discussion of the dependence of the sticking probability on the rotational state of the molecule, a topic of current experimental interest. The interest in this problem is due to the observation in electron energy loss and work function change measurements that there were different proportions of parahydrogen and orthohydrogen measured on the surface for the same exposure of each gas.[48] Subsequent molecular beam measurements of the sticking probability have borne out this observation in a surprising way; there are peaks in the sticking probability when the total energy of the incident molecule is equal to a rotational excitation.[49] Even more surprising are subsequent measurements of the elastic-scattering probability[50] that show features related to those seen in the sticking probability. The results of these experiments are difficult to understand in terms of the assumptions we make in these calculations, particularly difficult are the peaks that occur when the total energy of the particle is equal to a rotational transition energy.

Our earlier calculations for the trapping probability[13] showed that the rotational dependence of the sticking probability was not due to the selective adsorption resonance enhanced trapping because the resonances were extremely narrow and had a very small weight. In that calculation we used a form for the potential[24] that had a much weaker orientational dependence than found in subsequent calculations.[25] We used different phonon cutoffs, a larger value of ω_D and Q_c than we currently believe to be the most appropriate. Our potential choice led us to underestimate the differences due to the rotational degrees of freedom, and our choice of cutoffs leads to an overestimation of the effects of the selective adsorption resonances because it allowed resonances with higher energies to contribute to the trapping probability.

Figure 11 shows the results of a calculation for the probability for trapping onto a zero-temperature copper surface as a function of incident energy. The calculation was done for the molecules normally incident on the surface, and then the energy was scaled by $(\cos 60°)^{-2}$ to convert from the normal energy to the total energy for an angle of incidence of 60°, the experimental angle of incidence. For the approximations we make, using the energy in motion normal to the surface is sufficient to account for almost all of the effect of off-normal incidence on the inelastic-scattering probabilities. The curves for orthohydrogen and paradeuterium (both odd angular momentum species) have been averaged over the possible values of the azimuthal quantum number. For the values of the parameters used in this calculation there are no resonances that contribute to one-phonon trapping for H_2, and the ones that contribute for orthodeuterium are extremely weak. There are differences of about 10% between the even and odd angular momentum species of both H_2 and D_2 due to the differences in the angular momentum state matrix elements of the orientationally dependent potential. These 10% differences are probably below experimental resolution because the populations of para- and orthohydrogen in the two different gas mixtures are not that well known. The H_2 trapping probability is roughly twice that of D_2 at low energies, but at higher energies they are almost the same. The low-energy ratio of the experimentally measured deuterium sticking probability is larger than that of hydrogen by a factor of 2, but the ratio increases at higher energies rather than decreases. This increase in the ratio is understandable because multiphonon contributions (relative to the one-phonon contributions) to the trapping are more important for deuterium, since its mass is greater, than they are for hydrogen.

A trapping probability as calculated here is not a sticking probability that would be measured experimentally. A particle in a trapped state will not in general stay in that state because it is still coupled to the phonons, so a trapped state cannot be viewed as a proper final state in a scattering calculation. However, if the inelastic lifetime of a trapped state is longer than the scattering time, it makes sense to use such a trapping probability as input to a kinetic calculation of the sticking probability.[51] It also makes sense to treat trapping in this manner to study its effect on elastic scattering.

On the other hand, it is difficult to see how the experimental features can come out of such a combined trapping and kinetic calculation. This discrepancy indicates that scattering and trapping for low-energy, low-mass particles on cold surfaces may be more complicated than is consistent with the assumptions in such a distorted-wave perturbative approach.

2. *HD Static surface scattering*

The asymmetry of the HD molecule has two important consequences for the dependence of the scattering probabilities on the rotational degrees of freedom. (1) Since the nuclei are distinguishable, odd angular momentum transitions are allowed. (2) Since the center of mass is offset from the centroid of the electron cloud, the translational-rotational coupling is much stronger than it is for H_2 or D_2. The increased coupling to rotations gives much stronger rotationally inelastic scattering and much

broader selective adsorption resonances. These resonances are broad enough that they can be treated within the self-consistent one-phonon approximation developed in I which allows a quantitative calculation of resonant scattering for these systems leading to a qualitative understanding of the effect of inelastic scattering on selective adsorption resonances in other systems.

Features of HD scattering from noble metals that have been seen experimentally[52–55] are rotationally inelastic scattering with well-defined rotational transitions, selective adsorption resonances in the scattering probabilities, and variations in the temperature dependence of these quantities. While quantative comparisons with absolute scattering probabilities are difficult, all of the qualitative features of these experiments are described by the theory developed in I.

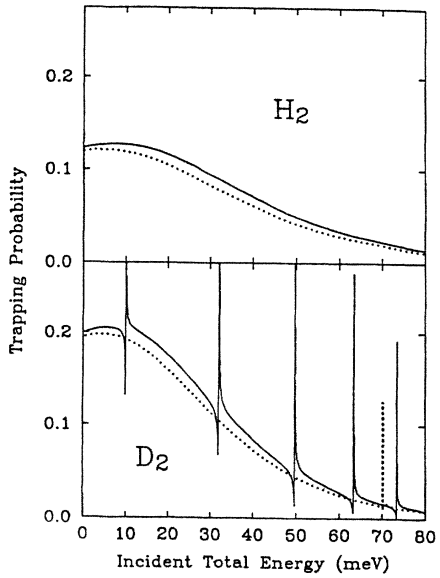

FIG. 11. The trapping probability for molecular-hydrogen scattering from copper. The top panel shows the trapping probability for H_2 and the bottom panel that for D_2 calculated in the distorted-wave Born approximation for scattering from a zero-degree copper surface for an incident angle of 60°. The calculation has been done for a normally incident molecule and then the incident energy adjusted to account for the off-normal incidence, since it was shown in Sec. II B of this paper that using the normal energy rather than the total energy accounts for almost all of the effects of off-normal incidence. The solid curves are the trapping probability for the $l=0$ incident rotational state molecules (parahydrogen and orthodeuterium) and the dotted curves are for the $l=1$ rotational states averaged over the azimuthal quantum number. Because of the mass ratio the D_2 trapping coefficients are a factor of 2 larger than those for H_2 except the highest energies where they are about the same. There are no selective adsorption resonances for H_2 in this energy regime, and those for D_2 are weak; even if the resonances were not weak in a distorted-wave Born approximation treatment, their effect on trapping would be reduced because all the inelastic-scattering probabilities are enhanced, so that the enhancement of each is reduced in a self-consistent calculation. These trapping probabilities cannot be directly compared to sticking coefficients but should be used as inputs to a kinetic calculation of sticking probabilities.

Figure 12 gives the scattering probability for HD scattering from a static (lattice atoms fixed) copper surface. The top panel shows the elastic, or $l=0$, scattering probability which is unity for all energies below 11 meV because there are no other accessible outgoing states. Above 11 meV the molecules can scatter from the surface into either the $l=0$ state or the rotationally inelastic $l=1$ state which is shown in the middle panel of the figure. The translational-rotational coupling is strong enough that most of the molecules scatter into the rotationally excited state. At the selective adsorption resonances the scattering probabilities change rapidly as a function of energy with the elastic-scattering probability approaching unity and the rotationally inelastic-scattering probability approaching zero. This rapid change in the scattering probabilities is due to the constructive and destructive interference between the directly scattering flux and the flux that has coupled back out of the rotationally trapped state. The bottom panel shows the occupation of the rotationally trapped states that lead to the selective adsorption resonances; below 11 meV the figure shows the probability density in the $l=1$ state, and above 11 meV it shows the probability density in the $l=2$ state. The probability density is calculated by integrating over all z the amplitude squared of the scattering state in the appropriate angular momentum channel of the scattering state.

The roughly Lorentzian peaks in the trapped probability density are better measures of the resonance widths than the Fano-like elastic-scattering line shapes because the shape of the latter obscures its width

$$P_{\rm el}(E_z)\approx P_{\rm background}\frac{[(E_z-E_r)-q]^2}{(E_z-E_r)^2+\Gamma^2}\ , \tag{3.10}$$

where Γ is the width of the resonance and q is a parameter that measures the asymmetry of the line shape. Because the line shapes are Fano-like there is structure in the resonance line shapes that extend over a larger range of energy than the width of the resonance. This Fano-like shape with a peak and dip in both channels is not a general expression for a selective adsorption resonance line shape; resonances can consist of isolated peaks or dips or even more complicated shapes.[56–59] This shape does, however, happen to describe these line shapes quite well over a small energy range that is nonetheless large compared to the width of the resonance.

The low-energy resonances are much broader than the higher-energy ones. The resonance widths depend on the matrix element of the off-diagonal parts of the potential [see Eq. (5.26) of I] with the bound states and the density of continuum states at the resonance energy. The overlap of the bound states with the off-diagonal parts of the potential, the largest part of which is due to the $l''=1$ term in the potential, is roughly equal to the product of the derivative of the diagonal part of the potential and the offset of the center of mass. While the lowest-bound state is centered near the well minimum where the derivative of the potential is small, the subsequent bound states penetrate further into the surface but also have more and

more of their amplitude centered far from the surface. Due to these conflicting trends the matrix element (for these potentials) tends to be largest for the second- and third-bound states. The density of states is larger the closer the rotationally deexcited state is to the vacuum since the density of states in one dimension (due to the flat-surface approximation, the parallel degrees of freedom decouple completely in this aspect of the problem) is inversely proportional to the square root of the kinetic energy of the scattering particle, $E^{-1/2}$. For resonances at energies high enough that there are several final states, the width depends on contributions from all possible final state, but the largest contribution is from the lowest-energy rotational deexcitation because the matrix element is larger (that term in the coupling potential is largest), and the density of states is largest for the rotational deexcitation that is closest to the vacuum.

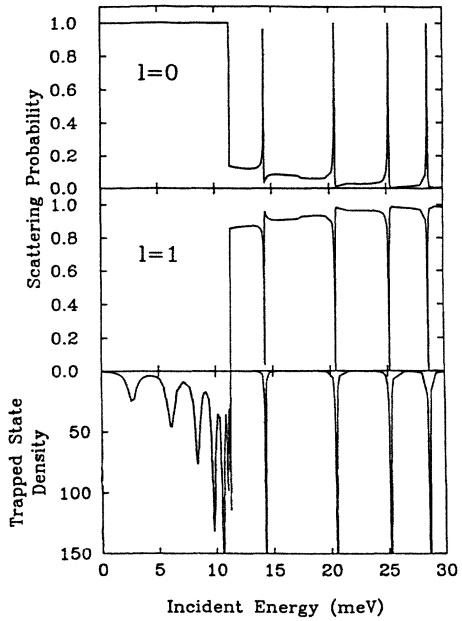

FIG. 12. HD-scattering probabilities from a static copper surface. The elastic- (top panel) and rotationally inelastic- (middle panel) scattering probabilities for HD scattering from a static copper at normal incidence are plotted as a function of the incident energy. The bottom panel shows the density in the rotationally excited trapped state integrated over the position normal to the surface also as a function of the incident energy. This quantity, a measure of the time spent near the surface in a rotationally excited state, is strongly peaked at the selective adsorption resonances. As seen in the middle panel, no molecules with incident energies below 11 meV leave the surface rotationally excited. For these energies $l=1$ rotational state can be resonant with the bound states of the surface potential as seen from the broad overlapping peaks in the bottom panel, but the elastic-scattering probability is not affected because there is only one final state. Above 11 meV the molecule can scatter into either an $l=0$ or an $l=1$ state and leave the surface, and the $l=2$ state can be resonant with the bound states giving selective adsorption resonances. Resonances for which there are more than one possible final state cause peaks in the elastic $l=0$ scattering probability and dips in the rotationally inelastic $l=1$ scattering probability as well as increased trapped state densities. Unlike the resonances for energies below 11 meV these resonances are much sharper and do not overlap each other.

3. *Finite temperature surface scattering*

Molecules can also scatter inelastically off a *dynamic* surface by exciting or absorbing a phonon. Inelastic scattering strongly affects the scattering resonances in Fig. 12, as is seen in Fig. 13 where scattering probabilities, calculated using the self-consistent one-phonon approximation discussed in I, are plotted as a function of incident energy for a series of surface temperatures. In these plots the resonances below 11 meV become observable in the elastic-scattering probability due to the enhanced inelastic scattering for molecules scattering under resonance conditions. The higher-energy resonances are all considerably broadened and damped by the inelastic scattering.

The apparent size of each low-energy resonance increases, with respect to the background, as a function of temperature. This somewhat surprising result—the resonances become easier to observe as the inelastic scattering increases—is due to two reasons. First, the resonances are observable only because the inelastic scattering provides additional channels for the particle flux besides the elastic channel. The enhanced inelastic scattering at the selective adsorption resonances in turn decreases the amount of elastic scattering making the resonances observable. Second, the elastic widths of the resonances are larger than the inelastic widths for all the temperatures shown in this plot as can be seen in the temperature independence of the trapped state density. Since the resonances do not broaden they have a larger and larger effect on the elastic scattering as the temperature increases. These resonances are very broad because they are both low in energy which couples them to a large density of continuum states and have a large matrix element with the translational-rotational coupling potential. Since the inelastic coupling is strongest between states with the same angular momentum the inelastic widths of the resonances do not depend as strongly on the energy of the resonances as the elastic widths do, because the matrix elements and the densities of states for those states are independent of the rotational state. In fact, the inelastic width of a resonance is dominated by coupling to the other bound states with the same angular momentum as is shown in Fig. 17. The inelastic width of the resonance is affected by which bound state is resonant in much the same way as the elastic lifetime is; it is the matrix element of the bound-state wave function with the derivative of the diagonal part of the potential (the inelastic interaction potential is proportional to the derivative of the static surface potential) that is important. For example, high-lying bound states have longer inelastic lifetimes than lower-lying ones.

The higher-energy resonances have a much narrower width than the lower-energy states so that the inelastic scattering affects the line shapes more strongly. The effect of inelastic scattering on one of the higher-energy resonances is shown in Fig. 13(b) which shows the resonances broadening and becoming less distinct as the sur-

face temperature (and hence inelastic scattering) increases. Using the width at half-maximum of the approximately Lorentzian trapped state density as a measure of the inverse lifetime or width of the resonance gives a change in width of roughly a factor of 2 between the zero-temperature and the 280 K surface and another factor of 2 between the static surface width and the zero-temperature width. For the resonance near 25 meV, for example, the static surface width is 0.08 meV, the 0 K width is 0.15 meV, and the 280 K width is 0.25 meV. As is discussed with respect to Eq. (3.9) the inverse of the static surface width gives the elastic lifetime of the resonance, and the inverse of the difference between the full width and the static surface width gives the inelastic lifetime of the resonance.

Since the inelastic width is determined by scattering to other states with the same angular momentum, the inelastic widths for the H_2 and D_2 resonances are likely to be very close to the inelastic widths found for the HD resonances that are due to bound states with roughly the same energy. Since these inelastic HD widths are much larger than the elastic widths found for the H_2 and D_2 resonances (the parahydrogen resonances around 25 meV have a width of 0.003 meV, while zero-temperature inelastic width for HD at the same energy is 0.07 meV), the total widths of the H_2 and D_2 resonances will be dominated by inelastic scattering rather than the translational-rotational coupling.

Thermal extrapolation. Calculations of scattering probabilities are most often done for scattering from a static surface, particularly if a series of potentials are to be evaluated as to which best matches the experimental data. To make this comparison it is necessary to take experimental data which is measured at a finite surface temperature and convert it into data that would be measured for scattering from a static surface. To study this procedure we use scattering probabilities calculated in the self-consistent one-phonon approximation as experimental data and use various extrapolation methods. Figure 14 shows the elastic and rotationally inelastic-scattering probabilities plotted on a logarithmic scale as a function of temperature for fixed energies. Although we only study HD scattering, this analysis can be generalized to the interpretation of diffraction intensities for helium scattering used as a structural probe.

Since the high-temperature limit of the mean-square displacement and the mean-square effective height extrapolate to zero at zero temperature rather than to their

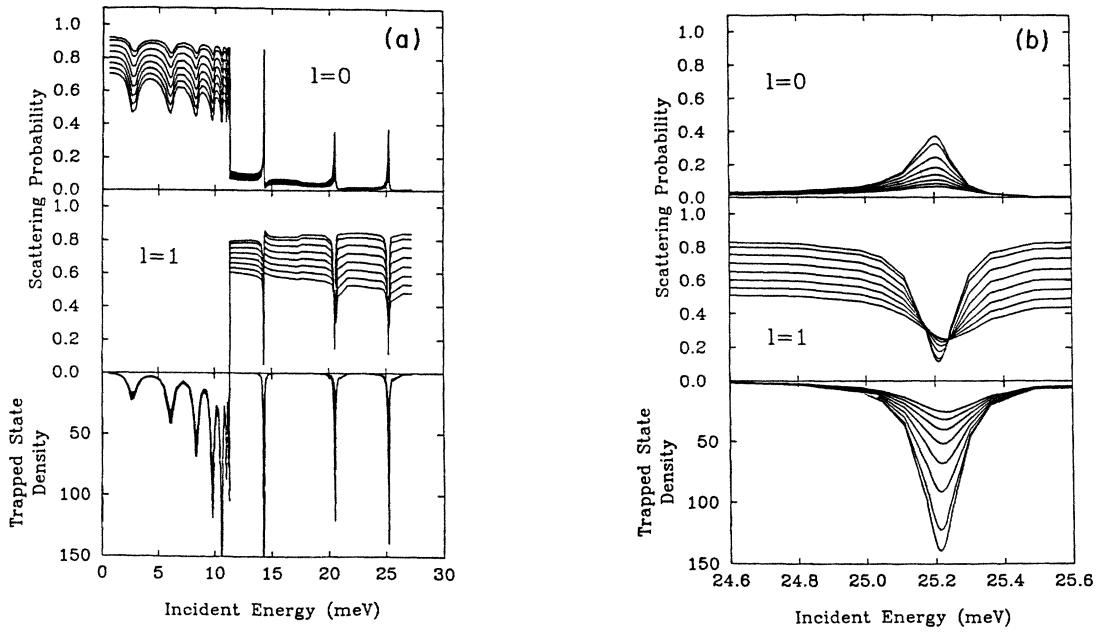

FIG. 13. (a) The energy dependence of HD scattering from copper. The elastic- (top panel), and rotationally inelastic- (middle panel) scattering probabilities for HD scattering from copper at normal incidence are plotted as a function of the incident energy for a series of eight temperatures between 0 and 280 K in increments of 40 K. The bottom panel shows the density in the rotationally excited trapped state integrated over the position normal to the surface. The shapes and sizes of these peaks are strongly affected by the inelastic scattering as can be seen by comparing these curves to each other and to the static surface scattering probabilities shown in Fig. 12. The resonances for energies below 11 meV, which are the dips in the elastic-scattering probability for scattering from a finite temperature surface but not apparent for scattering from a static surface, are only observable through the enhanced inelastic scattering caused by the resonances. (b) A detail of the scattering probabilities near a selective adsorption resonance. The elastic-scattering probability $l=0$ has a maximum, and the rotationally inelastic-scattering probability $l=1$, has a minimum due to a resonance. The maximum in the elastic scattering is strongly reduced by the inelastic scattering as the temperature increases (for a static surface the amplitude of the peak becomes very close to unity), while the minimum in the rotationally inelastic-scattering probability is less strongly affected. The trapped state probability is also strongly reduced by the inelastic scattering suggesting that the resonance width is dominated by the inelastic scattering rather than the translational-rotational coupling.

zero-temperature values, i.e., the extrapolation eliminates both thermal and zero-point-motion effects, it is not unreasonable to expect that the same type of extrapolation would work for elastic and rotationally inelastic-scattering probabilities. In particular, if a Debye-Waller factor or an exponentiated inelastic-scattering model describes the effect of inelastic scattering on elastic scattering, then the extrapolation of the logarithm of the scattering probability would give the static surface scattering probabilities exactly because in the high-temperature limit the argument of the exponential of these models is proportional to the temperature. We do not, however, expect such an extrapolation to work for resonant scattering conditions because these methods do not account for the effect of inelastic scattering on the resonance widths.

None of the scattering probabilities below 11 meV extrapolate back to unity, the static surface limit, which is not surprising since those resonances all overlap. The closer the energy is to the center of a resonance the further from unity the extrapolated value of the scattering probability is. Since the resonances above 11 meV are much narrower than those below and do not overlap, both the elastic and the rotationally inelastic-scattering probabilities shown in Fig. 13 extrapolate back to the static surface scattering values for nonresonant energies. Again, the resonant scattering probabilities do not extrapolate to the static surface values, and because inelastic scattering plays a much more important effect on the widths of these resonances, the extrapolations miss by a much greater amount than those for the lower-energy resonances. The extrapolation as a function of energy is given in Fig. 15 and is compared with the static surface scattering probabilities.

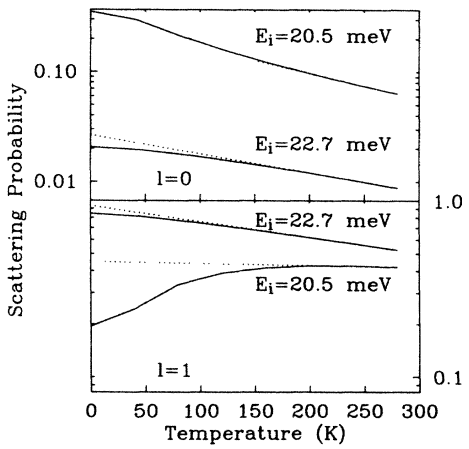

FIG. 14. Elastic- and rotationally inelastic-scattering probabilities as a function of temperature for HD scattering from copper. The top panel shows the elastic- ($l=0$) and bottom panel the rotationally inelastic-scattering probabilities as a function of temperature. The probabilities are plotted for a nonresonant and a resonant incident energy 22.7 meV and 20.5 meV, respectively. The dotted lines associated with each curve show the extrapolation of the high-temperature scattering probabilities to the static surface limit. These extrapolated values are shown in Fig. 15 as a function of incident energy.

Another possible way to convert finite-temperature data to the static surface limit that we evaluate is the use of Beeby-corrected Debye-Waller factor. The advantage of this type of extrapolation is that it can be done with data taken at a single temperature, whereas the previously discussed method required data at several temperatures. A Beeby-corrected Debye-Waller analysis of diffraction intensities predicts a temperature dependence given by

$$P_{\rm el}^{\rm BCDW} = \exp\{-2m[(E_z+D)^{1/2}+(E_x+D-E_{\rm rot})^{1/2}]^2 \times \langle h(\mathbf{R})^2\rangle_{th}\}\ , \tag{3.11}$$

where $E_{\rm rot}$ is the change in the rotational energy during the scattering process. The temperature dependence is in the mean-square effective height of the surface $\langle h(\mathbf{R})^2\rangle_{\rm th}$. A simple Debye-Waller analysis predicts the same general form for the temperature dependence without the addition of the well depth to the incident energy. The extrapolations of the high-temperature scattering probabilities using a Beeby-corrected Debye-Waller, also shown in Fig. 15, do not work as well as the extrapolations using calculated scattering probabilities for several temperatures. In fact they predict an incorrect overall energy dependence for the rotationally inelastic-scattering probability.

All the difficulties encountered using a Beeby-corrected Debye-Waller for analyzing temperature-dependent helium scattering from a flat surface discussed earlier in this chapter also persist for analyzing scattering in systems that allow rotationally inelastic scattering as can be seen in the roughly factor of 2 errors made in the total intensity. For these systems there is the additional question of whether inelastic scattering leads to rearrangement of scattering intensity between different rotational channels and whether the Debye-Waller factor correctly describes it. Figure 15 shows the ratio of the rotationally inelastic scattering and the elastic scattering for the static surface scattering probabilities to the same ratios for the extrapolated scattering probabilities and the Beeby-corrected Debye-Waller predictions for the static surface scattering probabilities. The agreement between the static surface values and the extrapolated values indicates that out of resonance rearrangement is temperature independent. The disagreement between the static surface values and the Beeby-corrected Debye-Waller values indicates that this later method incorrectly describes the differences in the elastic and rotationally inelastic scattering due to the loss in energy in motion normal to the surface. However, the Beeby-corrected Debye-Waller factor does account for roughly two-thirds of the difference between the ratio of the static surface scattering probabilities and the ratio of the finite-temperature scattering probabilities.

4. Densities and distributions

Much can be learned about the scattering process by examining the probability and flux densities as a function of distance from the surface as shown in Fig. 16. Comparison of the $l=2$ probability density of the resonantly scattering molecules with that for the nonresonantly

scattering molecules shows the large buildup in the rotationally trapped state for the resonantly scattering molecule. It should be kept in mind that these probabilities are plotted for scattering from an 80 K surface so that the probability density in the rotationally trapped state has been significantly reduced by inelastic scattering from its static surface value. The difference between this probability density and the static surface value (roughly a factor of 4) indicates why the distorted-wave Born breaks down at selective adsorption resonances. Because the amplitude in the rotationally trapped state is significantly decreased by the inelastic scattering, a calculation that ignores this effect (the inelastic contribution to the width or lifetime of the resonance) will overcount the inelastic scattering due to the selective adsorption resonance. This feature can also be seen in the bottom panels of Figs. 13 which show the integrated probability density in the rotationally trapped states for a series of temperatures.

While both the probability density and the flux density show that the molecule does not penetrate into the surface, the probability density can be difficult to interpret because the plane waves have unit normalization rather than flux normalization, and there are interference effects between incoming and outgoing waves in the incident channel. The flux density provides a more straightforward interpretation of the dynamics of the scattering process, because it shows directly where the scattering between the various channels occurs. The spatial location of the flux changes between the various channels show that for nonresonantly scattering molecules most of the rotationally inelastic and inelastic scattering takes place very close to the classical turning point. This fact justifies our use of the local-height approximation which is valid just where it needs to be valid to correctly describe the inelastic scattering—near the classical turning point. This narrow spatial region in which the scattering takes place is due to the molecular wave functions decaying rapidly into the surface and the potential decaying rapidly away from the surface.

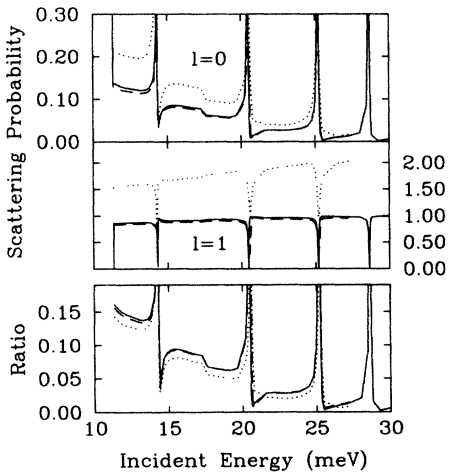

FIG. 15. A comparison of finite-temperature extrapolation predictions for elastic- and rotationally inelastic-scattering probabilities. The self-consistent one-phonon approximation results are analyzed as experimental data in two ways: (1) the log of the high-temperature scattering probabilities are extrapolated to zero temperature (dashed lines) and (2) the effects of inelastic scattering are accounted for by a Beeby-corrected Debye-Waller factor (dotted lines). These predictions are to be compared to the static surface scattering probability (solid lines). The top panel shows the elastic-scattering probability and the middle panel shows the rotationally inelastic-scattering probability. The bottom panel shows the ratio of the rotationally inelastic-scattering probability to the elastic-scattering probability for the static surface scattering probability and each of the methods used to analyze the high-temperature (calculated) data. While the agreement between the extrapolated predictions (dotted line) and the actual static surface results (solid line) is good for nonresonant scattering, there is a roughly 10% discrepancy between the Beeby-corrected Debye-Waller factor analyzed data (dashed line) and the static surface results.

For resonantly scattering molecules there is rearrangement of flux between channels much further from the surface, because the large build-up of probability in the rotationally trapped state seen in the $l=2$ probability density compensates for the weakness of the interaction potential at those distances. This rearrangement is probably not calculated quantitatively correctly because the local-height approximation is not as valid that far from the surface.

It is also possible to compute the distribution of the inelastic (one-phonon-change) flux far from the surface over the possible final states which is shown in Fig. 17 for both resonantly and nonresonantly scattering molecules. Here the distributions are plotted as a function of the change in energy in motion normal to the surface and are integrated over possible parallel momenta. For the flat surface potential model that we use in these calculations the full distribution over final states separates into a product of a factor that depends just on the change in the energy in motion normal to the surface and a factor that depends on both the change in that energy and the change in parallel momentum but not on any details of the state of the scattering molecule (only on the phonon density of states). This separability means that the integral over all parallel momenta of the final-state distribution still contains all the information about the scattering from the point of view of the molecule.

The most prominent features in Fig. 17 are the strongly enhanced resonant final states for the resonant initial state. The enhancement of the final-state resonances for the nonresonant initial state is much weaker than it is for the resonant initial state. These two features are due to the form of the interaction potential that couples the zero-phonon-change states with the one-phonon-change states; since the interaction potential is the derivative of the static surface potential, it couples states with the same angular momentum much more strongly than it does states with different angular momenta. This form also explains why the trapping probability is not as strongly enhanced by resonant scattering as inelastic scattering to other continuum states is, because the bound states tend to be predominantly lower angular momentum states than the resonantly trapped state. The trapping probability into each bound state can be seen as vertical bars in the left part of each figure.

Even though the self-consistent one-phonon approximation qualitatively describes the correct behavior of resonances coupled to inelastic scattering, Fig. 17 shows why it should not be trusted quantitatively. The problem is that inelastic scattering out of the resonant final states is not included in the approximation. The method would work quantitatively correctly if the resonant final states (or any small set of states) were not as strongly enhanced as they are. When the background value of the inelastic-scattering probability is small, the effect on the elastic scattering of multiphonon-change processes will be small; when the inelastic-scattering probability for resonant states is large and the resonant final states are strongly enhanced, the approximation breaks down. We tried to remedy this breakdown by including an optical potential in the Schrödinger equation for the one-phonon-change amplitudes, but, as might be expected given our inability to find an optical potential that could treat the effect of one-phonon-change inelastic scattering on the zero-phonon-change amplitude, we were unable to get this approximation to work.

There are also several features in this figure that seem generally applicable. (1) The phase difference between different angular momentum channels causes interference

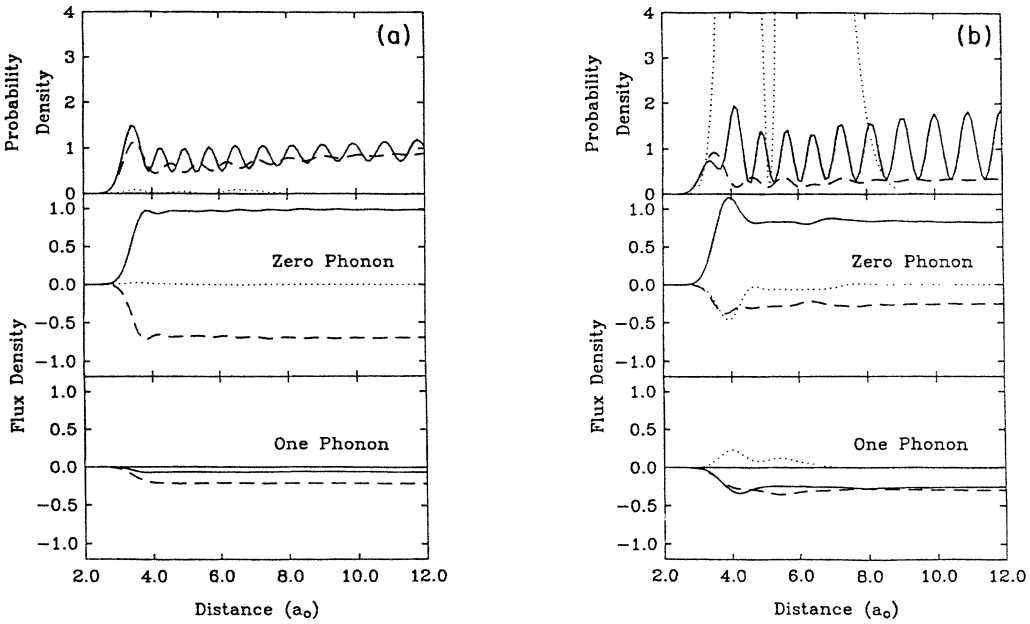

FIG. 16. (a) Probability and flux densities for HD scattering from copper out of resonance. The top panel shows the probability density of each angular momentum component of the wave function for which the phonons in the surface have not changed their state (the square of the zero-phonon-change amplitude) as a function of position. The HD molecule with a nonresonant energy of 22.7 meV is incident normally on the copper surface at 80 K. The incident part of the molecular wave function (as $l=0$ angular momentum state) beats against a much smaller amplitude outgoing wave in the same angular momentum state giving the oscillatory behavior in the solid curve. There is also an outgoing wave in the $l=1$ angular momentum state, but none in the $l=2$ because there is not enough energy in the incident particle to leave the surface in a state that highly rotationally excited. There is a slight average decrease in the probability in the potential well where the particle would be moving faster classically and a buildup of probability just before the classical turning point. That there is a net flux toward the surface is much easier to see in the lower two panels showing the flux density in each angular momentum state as a function of position. Positive values of the flux are net fluxes toward the surface and negative values are fluxes away from the surface. The solid line $l=0$ shows the unit incident flux and the almost imperceptible outgoing flux in that angular momentum state, and the dashed line $l=1$ shows the flux away from the surface in the rotationally excited part of the zero-phonon-change state. Finally, the bottom panel shows the inelastic flux, which is all away from the surface, in each angular momentum state integrated over all of the one-phonon-change states. Whereas the amplitudes of these states cannot be added together since different phonons have been excited, the flux densities can be. The distribution of flux between the different channels changes very close to the classical turning point implying that all of the rotational and inelastic scattering takes place at this point. Adding all the zero-phonon-change fluxes and the one-phonon-change fluxes together will give a net flux toward the surface, because there is flux lost to trapping in this model. (b) Probability and flux densities for resonant HD scattering from copper. This figure shows the same quantities as (a) except that the incident energy is the resonant energy 20.5 meV. The resonance is immediately apparent in the large probability density seen in the $l=2$ angular momentum state in the top panel. For this energy both the inelastic-scattering probability has increased as can be seen in the bottom panel and the elastic $l=0$ zero-phonon-change scattering probability has increased as can be seen in the increased amplitude of the oscillations in the $l=0$ zero-phonon-change probability density and in the deviation of the $l=0$ zero-phonon-change flux from one in the middle panel. The spatial location of the changes in the flux densities shows that the rotational and the inelastic scattering no longer just take place near the classical turning point but also further into the well where the buildup in probability density in the rotationally excited trapped state is large, and the derivative of the potential is still appreciable.

effects that change the line shape of the final-state resonances. (2) A related effect is that when there is a more than one possible angular momentum final state, the coupling seems to be strongest to the final state in which there is the strongest scattering in the static surface scattering problem. (3) There is a decrease in the final-state flux near the incident energy indicating that the matrix element for coupling to small-energy transfers is small because for finite temperatures the phonon matrix element is largest for small-energy transfers.

The self-consistent one-phonon approximation is useful for understanding the interaction between elastic-scattering effects and inelastic scattering, but since it is a one-phonon approximation it will not work quantitatively in situations such as selective adsorption resonances that are inherently multiphonon scattering dominated.

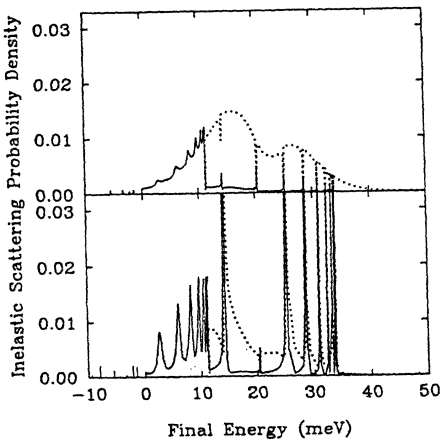

FIG. 17. Final-state scattering probabilities for HD scattering from copper. For the scattering conditions in the previous two plots, these two panels show the final-state distribution as a function of the *final* energy in both motion normal to the surface and in rotational motion integrated over all final parallel momenta. The top panel shows these quantities for a nonresonant incident energy 22.7 meV and the bottom panel for a resonant incident energy 20.5 meV. The solid curves are for molecules that leave the surface in the rotational ground state after scattering inelastically, and the dotted line is for the molecules that leave the surface rotationally excited after scattering inelastically. The short vertical lines in the lower right part of each panel give the trapping probability in each bound state of the surface potential. The top panel shows that most of the particles that scatter inelastically with final energies greater than 11 meV also scatter into a rotationally excited $l=1$ state. For the nonresonant incident state, the enhancement of inelastic scattering by resonant final states is small, but for the resonant incident state the final-state resonance enhancement is very large except for resonant states with energies close to the incident energy. The strong coupling between initial and final state resonance is due to the diagonal (in the angular momentum states of the scattering particle) elements of the interaction potential being much stronger than the off-diagonal elements, so that the large amplitude in the rotationally trapped state couples most strongly to the part of each final-state wave function with the same angular momentum.

IV. SUMMARY

In this paper we have used previously developed formal methods to calculate scattering probabilities for helium and molecular-hydrogen scattering from flat copper surfaces. We have developed a model for the interaction potential, calculated specific scattering probabilities, and made generalizations for other systems based on these results.

It is beyond current capabilities to calculate the interaction potential from first principles. To study the dynamics in these systems we have developed a procedure for extracting an approximate interaction potential for flat surfaces from the static surface potential. There are three general approximations: the flat surface approximation, the effective height approximation, and the attractive potential coupling. These approximations are the simplest that contain the essential features of the physics of scattering in these systems.

Using this interaction potential with no fitting parameters we found good quantitative agreement between experimental and calculated helium-scattering probabilities. We also found we could reproduce the essential features of HD scattering probabilities, including the behavior of the selective adsorption resonances. Within our model, however, it is not possible to explain the low-energy, low-surface temperature-scattering probabilities for molecular hydrogen.

Based on the agreement between theory and experiment we can generalize our results to other systems. In particular we showed how scattering will depend on the details of the potential such as the steepness and the well depth. Examination of the temperature dependence of selective adsorption resonances gives general rules for how inelastic scattering and selective adsorption resonances will effect each other depending on the relative contributions of elastic coupling and inelastic scattering to the width of the resonances. The temperatures dependence of the elastic- and rotationally inelastic-scattering probabilities shows that it should be possible to extrapolate finite-temperature diffraction probabilities to the static surface limit. This extrapolation allows the comparison of the data with scattering calculations to determine the potential.

ACKNOWLEDGMENTS

This work was supported by the U.S. Office of Naval Research. We thank Mats Persson and Cyrus Umrigar for numerous discussions and direct assistance with aspects of this calculation. We also thank both Horia Metiu for his hospitality during our stay in Santa Barbara and the Institute for Theoretical Physics where some of this manuscript was prepared.

*Present address: AT&T Bell Laboratories, Murray Hill, NJ 07974-2070.
[1]J. A. Barker and D. J. Auerbach, Surf. Sci. Rep. **4**, 1 (1985).
[2]G. Armand and J. R. Manson, Phys. Rev. Lett. **53**, 1112 (1984).
[3]G. Armand and J. R. Manson, in *Dynamics on Surfaces, 17th Proceedings of the Jerusalem Symposium on Quantum Chemistry and Biochemistry, 1984,* edited by B. Pullman, J. Jortner, A. Nitzan, and B. Gerber (Reidel, Dordrecht, 1984), p. 59.
[4]W. Brenig, Z. Phys. B **36**, 81 (1979).
[5]V. Bortolani, A. Franchini, F. Nizzoli, G. Santoro, G. Benedek, V. Celli, and N. Garcia, Solid State Commun. **48**, 1045 (1983), (He/Ag).
[6]R. G. Gordon, J. Chem. Phys. **51**, 14 (1969).
[7]J. R. Manson and V. Celli, Surf. Sci. **24**, 495 (1971).
[8]H.-D. Meyer and R. D. Levine, Chem. Phys. **85**, 189 (1984).
[9]J. Stutzki and W. Brenig, Z. Phys. B **45**, 49 (1981).
[10]M. Lagos, Surf. Sci. **65**, 124 (1977).
[11]J. Böheim, Surf. Sci. **148**, 463 (1984).
[12]D. Eichenauer and J. P. Toennies, in *Dynamics on Surfaces, 17th Proceedings of the Jerusalem Symposium on Quantum Chemistry and Biochemistry, 1984,* edited by B. Pullman, J. Jortner, A. Nitzan, and B. Gerber (Reidel, Dordrecht, 1984), p. 1.
[13]M. D. Stiles and J. W. Wilkins, Phys. Rev. Lett. **54**, 595 (1985).
[14]B. H. Choi and R. T. Poe, J. Chem. Phys. **83**, 1330 (1985).
[15]B. H. Choi and R. T. Poe, J. Chem. Phys. **83**, 1344 (1985).
[16]Y.-W. Lin and G. Wolken, J. Chem. Phys. **65**, 2634 (1976).
[17]Y.-W. Lin and G. Wolken, J. Chem. Phys. **65**, 3729 (1976).
[18]G. Wolken, J. Chem. Phys. **60**, 2210 (1974).
[19]M. Lagos and L. Birstein, Surf. Sci. **52**, 391 (1975).
[20]M. D. Stiles, J. W. Wilkins, and M. Persson, Phys. Rev. B **34**, 4490 (1986), hereafter referred to as I.
[21]V. Celli and A. A. Maradudin, Phys. Rev. B **31**, 825 (1985).
[22]J. Harris and P. Feibelman, Surf. Sci. **155**, 1133 (1982).
[23]C. Holmberg and P. Appell, Phys. Rev. B **30**, 5721 (1984).
[24]J. Harris and A. Leibsch, Phys. Scr. **14**, 14 (1983).
[25]P. Nordlander, C. Holmberg, and J. Harris, Surf. Sci. **152/153**, 702 (1985).
[26]P. Nordlander and J. Harris, J. Phys. C **17**, 1141 (1984).
[27]V. Bortolani, A. Franchini, N. Garcia, F. Nizzoli, and G. Santoro, Phys. Rev. B **28**, 7358 (1983).
[28]A. A. Maradudin and D. L. Mills, Ann. Phys. **100**, 262 (1976).
[29]A. A. Maradudin, in *Lattice Dynamics,* edited by M. Bulkanski (Flammarion, Paris, 1978), p. 284.
[30]R. B. Doak, U. Harten, and J. P. Toennies, Phys. Rev. Lett. **52**, 578 (1983), (He/Ag).
[31]U. Harten, J. P. Toennies, and C. Wöll, Faraday Discuss. Chem. Soc. **80**, 9 (1985), (He/Ag).
[32]H.-D. Meyer, Surf. Sci. **104**, 177 (1981).
[33]J. H. Weare, J. Chem. Phys. **61**, 2900 (1974).
[34]Z. W. Gortel, H. J. Kreuzer, and R. Teshima, Phys. Rev. B **22**, 512 (1980).
[35]G. Armand, J. R. Manson, and C. S. Jayanthi, Phys. Rev. B **34**, 6627 (1986).
[36]J. L. Beeby, J. Phys. C **4**, L359 (1971).
[37]J. Lapujoulade, Y. Lejay, and G. Armand, Surf. Sci. **95**, 107 (1980), (He/Cu).
[38]J. Lapujoulade, J. Perreau, and A. Kara, Surf. Sci. **129**, 59 (1983), (He/Cu).
[39]E. H. Conrad, D. S. Kaufman, L. R. Allen, R. M. Aten, and T. Engel, J. Chem. Phys. **83**, 5286 (1985), (He/Ni).
[40]A. Kaufold and J. P. Toennies, Solid State Phys. **173**, 320 (1986).
[41]M. Chiesa, L. Mattera, R. Musenich, and C. Salvo, Surf. Sci. **151**, L145 (1985), (H_2, D_2/Ag).
[42]J. M. Horne, S. C. Yerkes, and D. R. Miller, Surf. Sci. **93**, 47 (1980), (He,H_2/Ag).
[43]C.-F. Yu, K. B. Whaley, C. S. Hogg, and S. J. Sibener, Phys. Rev. Lett. **51**, 2210 (1983), (H_2/Ag).
[44]C.-F. Yu, K. B. Whaley, C. S. Hogg, and S. J. Sibener, J. Chem. Phys. **83**, 4217 (1985), (H_2/Ag).
[45]P. Cantini, S. Terreni, and C. Salvo, Surf. Sci. **109**, L491 (1981).
[46]P. Cantini and R. Tatarek, Surf. Sci. **114**, 471 (1983), (He/Gr).
[47]D. Evans, V. Celli, G. Benedek, J. P. Toennies, and R. B. Doak, Phys. Rev. Lett. **50**, 1854 (1984), (He/LiF).
[48]S. Andersson and J. Harris, Phys. Rev. B **27**, 9 (1983), (H_2/Cu).
[49]S. Andersson, L. Wilzén, and J. Harris, Phys. Rev. Lett. **55**, 2591 (1985), (H_2/Cu).
[50]S. Andersson, L. Wilzén, and J. Harris, Phys. Rev. Lett. **57**, 1603 (1986).
[51]W. Brenig, Z. Phys. B **48**, 127 (1982).
[52]J. P. Cowin, C.-F. Yu, S. J. Sibener, C. S. Hogg, and L. Wharton, in *Many-body Phenomena at Surfaces,* edited by D. Langreth and H. Suhl (Academic, Orlando, 1984), p. 351, (HD/Ag).
[53]K. B. Whaley, C.-F. Yu, C. S. Hogg, J. C. Light, and S. J. Sibener, J. Chem. Phys. **83**, 4235 (1985), (HD/Ag).
[54]C.-F. Yu, C. S. Hogg, J. P. Cowin, K. B. Whaley, J. C. Light, and S. J. Sibener, Isr. J. Chem. **22**, 305 (1982), (HD/Ag).
[55]U. Harten, J. P. Toennies, and Ch. Wöll, J. Chem. Phys. **85**, 2249 (1986).
[56]V. Celli, A. M. Marvin, and G. Benedek, Surf. Sci. **148** 54 (1984).
[57]W. L. Nichols and J. H. Weare, Phys. Rev. Lett. **56**, 753 (1986).
[58]K. L. Wolfe and J. H. Weare, Phys. Rev. Lett. **41**, 1663 (1978).
[59]V. Celli, in *Dynamics of Gas-Surface Interaction,* edited by G. Benedek and U. Valbusa (Springer-Verlag, Berlin, 1982), p. 2.